Background-free search for neutrinoless double beta decay with GERDA

(GERDA collaboration)[a]

M. Agostini,[1] M. Allardt,[4] A.M. Bakalyarov,[13] M. Balata,[1] I. Barabanov,[11] L. Baudis,[19] C. Bauer,[7] E. Bellotti,[8,9] S. Belogurov,[12,11] S.T. Belyaev,[13,b] G. Benato,[19] A. Bettini,[16,17] L. Bezrukov,[11] T. Bode,[15] D. Borowicz,[3,5] V. Brudanin,[5] R. Brugnera,[16,17] A. Caldwell,[14] C. Cattadori,[9] A. Chernogorov,[12] V. D'Andrea,[1] E.V. Demidova,[12] N. Di Marco,[1] A. di Vacri,[1] A. Domula,[4] E. Doroshkevich,[11] V. Egorov,[5,c] R. Falkenstein,[18] O. Fedorova,[11] K. Freund,[18] N. Frodyma,[3] A. Gangapshev,[11,7] A. Garfagnini,[16,17] C. Gooch,[14] P. Grabmayr,[18] V. Gurentsov,[11] K. Gusev,[5,13,15] J. Hakenmüller,[7] A. Hegai,[18] M. Heisel,[7] S. Hemmer,[16,17] W. Hofmann,[7] M. Hult,[6] L.V. Inzhechik,[11,d] J. Janicskó Csáthy,[15] J. Jochum,[18] M. Junker,[1] V. Kazalov,[11] T. Kihm,[7] I.V. Kirpichnikov,[12] A. Kirsch,[7] A. Kish,[19] A. Klimenko,[7,5,c] R. Kneißl,[14] K.T. Knöpfle,[7] O. Kochetov,[5] V.N. Kornoukhov,[12,11] V.V. Kuzminov,[11] M. Laubenstein,[1] A. Lazzaro,[15] V.I. Lebedev,[13] B. Lehnert,[4] H.Y. Liao,[14] M. Lindner,[7] I. Lippi,[17] A. Lubashevskiy,[7,5] B. Lubsandorzhiev,[11] G. Lutter,[6] C. Macolino,[1] B. Majorovits,[14] W. Maneschg,[7] E. Medinaceli,[16,17] M. Miloradovic,[19] R. Mingazheva,[19] M. Misiaszek,[3] P. Moseev,[11] I. Nemchenok,[5,c] D. Palioselitis,[14] K. Panas,[3] L. Pandola,[2] K. Pelczar,[3] A. Pullia,[10] S. Riboldi,[10] N. Rumyantseva,[5] C. Sada,[16,17] F. Salamida,[9] M. Salathe,[7] C. Schmitt,[18] B. Schneider,[4] S. Schönert,[15] J. Schreiner,[7] O. Schulz,[14] A.-K. Schütz,[18] B. Schwingenheuer,[7] O. Selivanenko,[11] E. Shevchik,[5] M. Shirchenko,[5] H. Simgen,[7] A. Smolnikov,[5,7] L. Stanco,[17] L. Vanhoefer,[14] A.A. Vasenko,[12] A. Veresnikova,[11] K. von Sturm,[16,17] V. Wagner,[7] M. Walter,[19] A. Wegmann,[7] T. Wester,[4] C. Wiesinger,[15] M. Wojcik,[3] E. Yanovich,[11] I. Zhitnikov,[5] S.V. Zhukov,[13] D. Zinatulina,[5] K. Zuber,[4] and G. Zuzel[3]

[1] *INFN Laboratori Nazionali del Gran Sasso and Gran Sasso Science Institute, Assergi, Italy*
[2] *INFN Laboratori Nazionali del Sud, Catania, Italy*
[3] *Institute of Physics, Jagiellonian University, Cracow, Poland*
[4] *Institut für Kern- und Teilchenphysik, Technische Universität Dresden, Dresden, Germany*
[5] *Joint Institute for Nuclear Research, Dubna, Russia*
[6] *European Commission, JRC-Geel, Geel, Belgium*
[7] *Max-Planck-Institut für Kernphysik, Heidelberg, Germany*
[8] *Dipartimento di Fisica, Università Milano Bicocca, Milan, Italy*
[9] *INFN Milano Bicocca, Milan, Italy*
[10] *Dipartimento di Fisica, Università degli Studi di Milano e INFN Milano, Milan, Italy*
[11] *Institute for Nuclear Research of the Russian Academy of Sciences, Moscow, Russia*
[12] *Institute for Theoretical and Experimental Physics, Moscow, Russia*
[13] *National Research Centre "Kurchatov Institute", Moscow, Russia*
[14] *Max-Planck-Institut für Physik, Munich, Germany*
[15] *Physik Department and Excellence Cluster Universe, Technische Universität München, Germany*
[16] *Dipartimento di Fisica e Astronomia dell'Università di Padova, Padua, Italy*
[17] *INFN Padova, Padua, Italy*
[18] *Physikalisches Institut, Eberhard Karls Universität Tübingen, Tübingen, Germany*
[19] *Physik Institut der Universität Zürich, Zurich, Switzerland*

(Dated: February 19, 2017)

Many extensions of the Standard Model explain the dominance of matter over antimatter in our Universe by neutrinos being their own anti-particles. This would imply that a lepton number violating radioactive decay named neutrinoless double beta ($0\nu\beta\beta$) decay exists whose detection requires utmost suppression of backgrounds. The GERDA collaboration searches for $0\nu\beta\beta$ decay of ^{76}Ge by operating bare detectors made from germanium with enriched ^{76}Ge fraction in liquid argon. Here, we report the first data of GERDA Phase II. A background level of $\sim 10^{-3}$ cts/(keV $\cdot$ kg $\cdot$ yr) has been achieved. Combining Phase I and II data, we find no signal and deduce a lower limit for the half-life of $5.3{\cdot}10^{25}$ yr at 90 % C.L. Our sensitivity of $4.0{\cdot}10^{25}$ yr is competitive with the best experiments that use significantly larger isotope mass. GERDA will be background-free up to its design exposure due to an active veto system, superior germanium detector energy resolution and improved background recognition of our new detectors. The potential of an essentially background-free search for $0\nu\beta\beta$ decay motivates a larger germanium experiment with higher sensitivity.

PACS numbers: 23.40.-s, 21.10.Tg, 27.50.+e, 29.40.Wk
Keywords: $0\nu\beta\beta$ decay, $T^{0\nu}_{1/2}$, ^{76}Ge, enriched Ge detectors, active veto

INTRODUCTION

One of the most puzzling aspects of cosmology is the unknown reason for the dominance of matter over anti-matter in our Universe. Within the Standard Model of

particle physics there is no explanation for this observation and hence a new mechanism has to be responsible. A favored model called leptogenesis [1] links the matter dominance to the nature of neutrinos and to the violation of lepton number, i.e. the total number of electrons, muons, taus and neutrinos minus the number of their anti-particles.

In most extensions of the Standard Model [2–4] neutrinos are assumed to be their own anti-particles (Majorana particles). This might lead to lepton number violating processes at the TeV energy scale observable at the LHC [4] and would result in neutrinoless double beta ($0\nu\beta\beta$) decay where a nucleus of mass number A and charge Z decays as $(A, Z) \rightarrow (A, Z + 2) + 2\,e^-$. Lepton number violation has not been unambiguously observed so far; indeed, its observation would motivate fundamental modifications of the Standard Model. There are several experimental $0\nu\beta\beta$ decay programs ongoing using for example ^{76}Ge [5, 6], ^{130}Te [7, 8] or ^{136}Xe [9–11]. They all measure the sum of the electron energies released in the decay which corresponds to the mass difference $Q_{\beta\beta}$ of the two nuclei. The $0\nu\beta\beta$ decay half-life is at least 15 orders of magnitude longer than the age of the universe. Its observation requires therefore the best suppression of backgrounds.

In the GERmanium Detector Array (GERDA) experiment bare germanium detectors are operated in liquid argon (LAr). The detectors are made from germanium with the ^{76}Ge isotope fraction enriched from 7.8 % to about 87 %. Since source and detector of $0\nu\beta\beta$ decay are identical in this calorimetric approach the detection efficiency is high.

This paper presents the first result from GERDA Phase II. In the first phase of data taking (Phase I), a limit of $T^{0\nu}_{1/2} > 2.1 \cdot 10^{25}$ yr (90 % C.L.) was found [5] for an exposure of 21.6 kg·yr and a background of 0.01 cts/(keV · kg · yr) at $Q_{\beta\beta} = (2039.061 \pm 0.007)$ keV [12]. At that time, the result was based on data from 10 detectors (17.6 kg total mass). In December 2015, Phase II started with 37 detectors (35.6 kg) from enriched material. The mass is hence doubled relative to Phase I. The ambitious goal is an improvement of the half-life sensitivity to $> 10^{26}$ yr for about 100 kg·yr exposure by reducing the background level by an order of magnitude. The latter is achieved by vetoing background events through the detection of their energy deposition in the LAr and the characteristic time profile of their signals in the germanium detectors. Up to the design exposure, the average expected background contribution is less than 1.0 in the energy region of interest ($Q_{\beta\beta}\pm0.5$ FWHM), defined according to the full width at half maximum (FHWM) energy resolution. This implies that GERDA will be the first "background-free" experiment in the field.

We will demonstrate in this paper that GERDA has reached the envisioned background level which is the world-best level if weighted by our superior energy resolution. GERDA is therefore best suited to not only quote limits but to identify with high confidence a $0\nu\beta\beta$ signal.

THE EXPERIMENT

The GERDA experiment [13] is located at the underground Laboratori Nazionali del Gran Sasso (LNGS) of INFN, Italy. A rock overburden of about 3500 m water equivalent removes the hadronic components of cosmic ray showers and reduces the muon flux at the experiment by six orders of magnitude to 1.2 $\mu/(\mathrm{m}^2\cdot\mathrm{h})$.

The pioneering feature of GERDA is the operation of bare germanium detectors in a radiopure cryogenic liquid like LAr for cooling to their operating temperature of ∼90 K and for shielding against external radiation originating from the walls (see Extended Data Fig. 1 for a sketch of the setup) [14]. In GERDA, a 64 m^3 LAr cryostat is inside a 590 m^3 water tank. The clean water completes the passive shield. Above the water tank is a clean room with a glove box and lock for the assembly of germanium detectors into strings and the integration of the liquid argon veto system.

GERDA deploys 7 coaxial detectors from the former Heidelberg-Moscow [15] and IGEX [16] experiments and 30 Broad Energy (BEGe) detectors [17]. All are produced from p-type material (see Extended Data Fig. 2). Electron-hole pairs created in the 1–2 mm thick n+ electrode mostly recombine such that the active volume is reduced. A superior identification of the event topology and hence background rejection is available for the BEGe type (see below). The enriched detectors are assembled into 6 strings surrounding the central one which consists of three coaxial detectors of natural isotopic composition. Each string is inside a nylon cylinder (see Extended Data Fig. 3) to limit the LAr volume from which radioactive ions like ^{42}K can be collected to the outer detector surfaces [18].

All detectors are connected to custom made low radioactivity charge sensitive amplifiers [19] (30 MHz bandwidth, 0.8 keV FWHM resolution) located in the LAr about 35 cm above the detectors. The charge signal traces are digitized with 100 MHz sampling rate and stored on disk for offline analysis.

In background events some energy is often also deposited in the argon. The resulting scintillation light [20] can be detected to veto them. In Phase II, a cylindrical volume of 0.5 m diameter and 2.2 m height around the detector strings (see Extended Data Fig. 1 and 4) is instrumented with light sensors. The central 0.9 m of the cylinder are defined by a curtain of wavelength shifting fibers which surround the 0.4 m high detector array. The fibers are read-out at both ends with 90 silicon photomulipliers (SiPM) [21]. Groups of six 3×3 mm^2 SiPMs are connected together to a charge sensitive amplifier.

Sixteen 3" low-background photomultpliers (PMT) designed for cryogenic operation are mounted at the top and bottom surfaces of the cylindrical volume. The distance to any germanium detector is at least 0.7 m to limit the PMT background contribution from their intrinsic Th/U radioactivity. All LAr veto channels are digitized and read-out together with the germanium channels if at least one detector has an energy deposition above ∼100 keV.

The nylon cylinders, the fibers, the PMTs and all surfaces of the instrumented LAr cylindrical volume are covered with a wavelength shifter to shift the LAr scintillation light from 128 nm to about 400 nm to match the peak quantum efficiency of the PMTs and the absorption maximum of the fibers.

The water tank is instrumented with 66 PMTs to detect Cherenkov light from muons passing through the experiment. On top of the clean room are three layers of plastic scintillator panels covering the central 4×3 m^2 to complete the muon veto [22].

DATA ANALYSIS

The data analysis flow is very similar to that of Phase I. The offline analysis of the digitized germanium signals is described in Refs. [5, 23, 24].

A data blinding procedure is again applied. Events with a reconstructed energy in the interval $Q_{\beta\beta} \pm 25$ keV are not analyzed but only stored on disk. After the entire analysis chain has been frozen, these blinded events have been processed.

The gain stability of each germanium detector is continuously monitored by injecting charge pulses (test pulses) into the front-end electronics with a rate of 0.05 Hz. The test pulses are also used to monitor leakage current and noise. Only data recorded during stable operating conditions (e.g. gain stability better than 0.1 %) are used for the physics analysis. This corresponds to about 85 % of the total data written on disk.

Signals originated from electrical discharges in the high voltage line or bursts of noise are rejected during the offline event reconstruction by a set of multi-parametric cuts based on the flatness of the baseline, polarity and time structure of the pulse. Physical events at $Q_{\beta\beta}$ are accepted with an efficiency larger than 99.9 % estimated with γ lines in calibration data, test pulse events and template signals injected in the data set. Conversely, a visual inspection of all events above 1.6 MeV shows that no unphysical event survives the cuts.

The energy deposited in a germanium detector is reconstructed offline with an improved digital filter [25], whose parameters are optimized for each detector and for several periods. The energy scale and resolution are determined with weekly calibration runs with ^{228}Th sources. The long-term stability of the scale is assessed by monitoring the shift of the position of the 2615 keV peak between consecutive calibrations. It is typically smaller than 1 keV for BEGe detectors and somewhat worse for some coaxial ones. The FWHM resolution at 2.6 MeV is between 2.6–4.0 keV (mean 3.2 keV, rms 0.4 keV) for BEGe and 3.4–4.4 keV (mean 3.8 keV, rms 0.3 keV) for coaxial detectors. The width of the strongest γ lines in the physics data (1460 keV from ^{40}K and 1525 keV from ^{42}K) is found to be 0.5 keV larger than the expectation for the coaxial detectors (see Fig. 1) likely due to gain instabilities in the corresponding read-out channels between calibrations. In order to conservatively estimate the expected energy resolution at $Q_{\beta\beta}$ an additional noise term is added to take this into account.

For $0\nu\beta\beta$ decays in the active part of a detector volume, the total energy of $Q_{\beta\beta}$ is detected in 92 % of the cases in this detector. Multiple detector coincidences are therefore discarded as background events. Two consecutive candidate events within 1 ms are also rejected (dead time $\sim10^{-4}$) to discriminate time-correlated decays from primordial radioisotopes, as e.g. the radon progenies ^{214}Bi and ^{214}Po. Candidate events are also rejected if a muon trigger occurred within 10 µs prior to a germanium detector trigger. More than 99 % of the muons that deposit energy in a germanium detector are rejected this way. The induced dead time is <0.1 %.

The traces from PMTs and SiPMs are analyzed offline to search for LAr scintillation signals in coincidences with a germanium detector trigger. An event is rejected if any of the light detectors record a signal of amplitude above 50 % of the expectation for a single photo-electron within 5 µs from the germanium trigger. About 99 % of the photons occur in this window. Accidental coincidences between the LAr veto system and germanium detectors create a dead time of (2.3 ± 0.1) % which is measured with test pulse events and cross checked with the counts in the ^{40}K peak. As the 1460 keV γ is produced by electron capture of ^{40}K, there is no residual energy that can be released in the LAr volume.

Fig. 2 shows the energy spectra for BEGe and coaxial detectors of Phase II with and without the LAr veto cut. Below ∼500 keV the spectra are dominated by ^{39}Ar β decays, up to 1.7 MeV by events from double beta decay with two neutrino emission ($2\nu\beta\beta$), above 2.6 MeV by α decays on the detector surface and around $Q_{\beta\beta}$ by a mixture of α events, ^{42}K β decays and those from the decays of the ^{238}U and ^{232}Th chains. The two spectra are similar except for the number of α events which is on average higher for coaxial detectors. The number of α counts shows a large variation between the detectors. The power of the LAr veto is best demonstrated by the ^{42}K line at 1525 keV which is suppressed by a factor ∼5 (see inset) due to the β particle depositing up to 2 MeV energy in the LAr. The figure also shows the predicted $2\nu\beta\beta$ spectrum from ^{76}Ge using our Phase I result for the half-life of $T^{2\nu}_{1/2} = (1.926 \pm 0.094) \cdot 10^{21}$ yr [26].

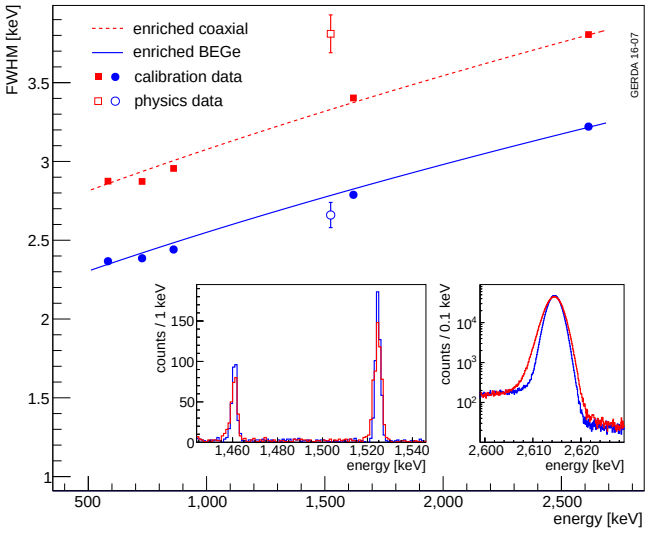

FIG. 1. — *energy scale and resolution* — Average energy resolution (FWHM) for γ lines of the calibration spectrum (filled symbols) and for the average of ^{40}K and ^{42}K lines from physics data (open symbols) for BEGe (symbols and solid line in blue) and coaxial (symbols and dashed line in red) detectors; the uncertainties (± 1 s.d.) are derived from the fit. The insets show the potassium lines and the 2615 keV calibration peak.

The time profile of the germanium detector current signal is used to discriminate $0\nu\beta\beta$ decays from background events. While the former have point-like energy deposition in the germanium (single site events, SSE), the latter have often multiple depositions (multi site events, MSE) or depositions on the detector surface. The same pulse shape discrimination (PSD) techniques of Phase I [27] are applied.

Events in the double escape peak (DEP) and at the Compton edge of 2615 keV photons in calibration data have a similar time profile as $0\nu\beta\beta$ decays and are hence proxies for SSE. These samples are used to define the PSD cuts and the related detection efficiencies. The latter are cross checked with $2\nu\beta\beta$ decays.

The geometry of BEGe detectors allows to apply a simple mono-parametric PSD based on the maximum of the detector current pulse A normalized to the total energy E [28, 29]. The energy dependence of the mean and the resolution σ_{ae} of A/E are measured for every detector with calibration events. After correcting for these dependences and normalizing the mean A/E of DEP events to 1, the acceptance range is determined for each detector individually: the lower cut is set to keep 90 % of DEP events and the upper position is twice the low-side separation from 1. Fig. 3 shows a scatter plot of the PSD parameter $\zeta = (A/E - 1)/\sigma_{ae}$ versus energy and the projection to the energy axis. Events marked in red survive the PSD selection. A survival fraction of (85^{+2}_{-1}) % is determined for $2\nu\beta\beta$ events which dominate the low energy part of the spectrum. The two potassium peaks and Compton scattered photons are reconstructed at $A/E < 1$ (below the SSE band). All 234 α events at higher energies exhibit $A/E > 1$ and are easily removed. The average $0\nu\beta\beta$ survival fraction is (87 ± 2) % [30]. The uncertainty takes into account the systematic difference between the A/E centroids of DEP and $2\nu\beta\beta$ events and different fractions of MSE in DEP and $0\nu\beta\beta$ events.

For coaxial detectors a mono-parametric PSD is not sufficient since SSE do not have a simple signature [27]. Instead two neural network algorithms are applied to discriminate SSE from MSE and from α surface events. The first one is identical to the one used in Phase I. The cut on the neural network qualifier is set to yield a survival fraction of DEP events of 90 % for each detector. For the determination of the $0\nu\beta\beta$ efficiency, $2\nu\beta\beta$ events in physics data and a complete Monte Carlo simulation [31] of physics data and calibration data are used. The simulation considers the detector and the electronics response to energy depositions including the drift of charges in the crystal [32]. We find a survival fraction for $0\nu\beta\beta$ events of (85 ± 5) % where the uncertainty is derived from variations of the simulation parameters.

The second neural network algorithm is applied for the first time and identifies surface events on the p+ electrode. Training is done with physics data from two different energy intervals. After the LAr veto cut events in the range 1.0–1.3 MeV are almost exclusively from $2\nu\beta\beta$ decay and hence signal-like. Events above 3.5 MeV are almost all from α decays on the p+ electrode and represent background events in the training. As $0\nu\beta\beta$ efficiency we measure a value of (93 ± 1) % for a $2\nu\beta\beta$ event sample not used in the training. The combined PSD efficiency for coaxial detectors is (79 ± 5) %.

RESULTS

This analysis includes the data sets used in the previous publication [5, 33], an additional coaxial detector period from 2013 (labeled "PI extra") and the Phase II data from December 2015 until June 2016 (labeled "PIIa coaxial" and "PIIa BEGe"). Table I lists the relevant parameters for all data sets. The exposures in the active volumes of the detectors for ^{76}Ge are 234 and 109 mol·yr for Phase I and II, respectively. The efficiency ϵ is the product of the ^{76}Ge isotope fraction (87 %), the active volume fraction (87–90 %), the $0\nu\beta\beta$ event fraction reconstructed at full energy in a single crystal (92 %), pulse shape selection (79–92 %) and the live time fraction (97.7 %). For the Phase I data sets the event selection including the PSD classification is unchanged. An improved energy reconstruction [25] is applied to the data as well as an updated value for the coaxial detector PSD efficiency of the neural network analysis of (83 ± 3) % [31].

Fig. 4 shows the spectra for the combined Phase I data

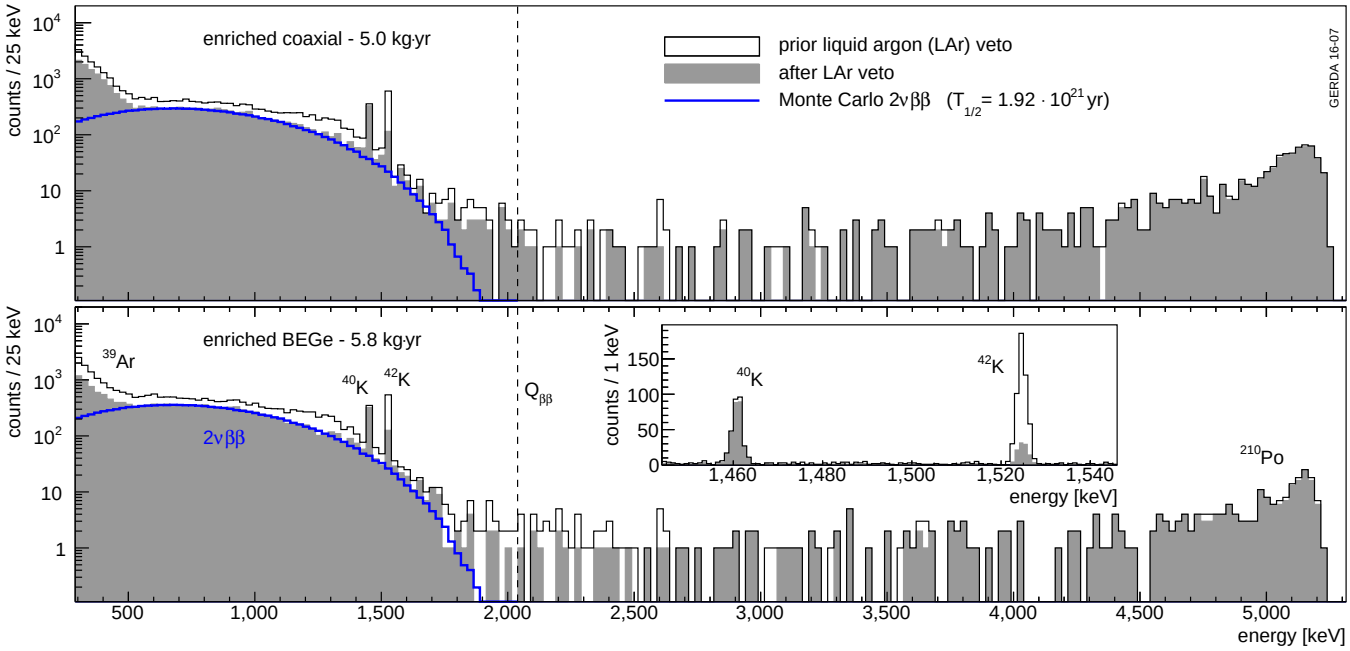

FIG. 2. — *energy spectra for the two detector types* — Energy spectra of Phase II data sets before (open histogram) and after argon veto cut (filled histogram). The blue lines are the expected $2\nu\beta\beta$ spectra from our recent half-life measurement. The inset shows the BEGe spectrum in the energy region around the two potassium lines. Note, the ^{40}K line is not suppressed since no energy is deposited in the LAr. Various background contributions are labeled in the bottom panel.

TABLE I. — *parameters of data sets* — List of data sets, exposures $\mathcal{E}$ (for total mass), energy resolutions in FWHM, efficiencies ϵ (including enrichment, active mass, selection efficiencies and dead times) and background indices (BI) in the analysis window excluding $Q_{\beta\beta}\pm5$ keV.

data set	$\mathcal{E}$ [kg·yr]	FWHM [keV]	ϵ	BI 10^{-3}cts/(keV · kg · yr)
PI golden	17.9	4.3(1)	0.57(3)	11 ± 2
PI silver	1.3	4.3(1)	0.57(3)	30 ± 10
PI BEGe	2.4	2.7(2)	0.66(2)	5^{+4}_{-3}
PI extra	1.9	4.2(2)	0.58(4)	5^{+4}_{-3}
PIIa coaxial	5.0	4.0(2)	0.53(5)	$3.5^{+2.1}_{-1.5}$
PIIa BEGe	5.8	3.0(2)	0.60(2)	$0.7^{+1.1}_{-0.5}$

sets and the two Phase II sets. The analysis range is from 1930 to 2190 keV without the intervals (2104 ± 5) keV and (2119 ± 5) keV of known peaks predicted by our background model [18]. For the Phase II coaxial detectors four events survive the cuts which means that the background is reduced by a factor of three compared to Phase I (see "PI golden" in Tab. I). Due to the better PSD performance, only one event remains in the BEGe data which corresponds to a background of $0.7^{+1.1}_{-0.5} \cdot 10^{-3}$ cts/(keV·kg·yr). Consequently, the Phase II background goal is reached.

The statistical analysis is described in the Extended Method section. We perform both a frequentist and a Bayesian analysis based on an unbinned extended likelihood function [33]. The fit function for every data set is a flat distribution for the background (one free parameter per data set) and for a possible signal a Gaussian centered at $Q_{\beta\beta}$ with a width according to the corresponding resolution listed in Table I. The signal strength is calculated for each set according to its exposure, efficiency and the inverse half-life $1/T$ which is a common free parameter. The analysis accounts for the systematic uncertainties due to efficiencies and energy resolutions (see Table I), and to a possible offset in the energy scale.

The p-value distribution for the frequentist analysis is shown in the Extended Data Fig. 5. The best fit yields zero signal events and a 90 % C.L. limit of 2.0 events in 34.4 kg·yr total exposure or

$$T^{0\nu}_{1/2} > 5.3 \cdot 10^{25}\,\text{yr}. \quad (1)$$

The (median) sensitivity assuming no signal is $4.0 \cdot 10^{25}$ yr. The systematic uncertainties weaken the limit by <1 %.

The Bayesian fit yields for a prior flat in $1/T$ between 0 and 10^{-24} /yr a limit of $T^{0\nu}_{1/2} > 3.5 \cdot 10^{25}$ yr (90 % C.I.). The sensitivity assuming no signal is $3.1 \cdot 10^{25}$ yr.

DISCUSSION

GERDA Phase II has been taking data since December 2015 in stable conditions with all channels working. The background at $Q_{\beta\beta}$ for the BEGe detectors is $(0.7^{+1.1}_{-0.5}) \cdot 10^{-3}$ cts/(keV · kg · yr). This is a major

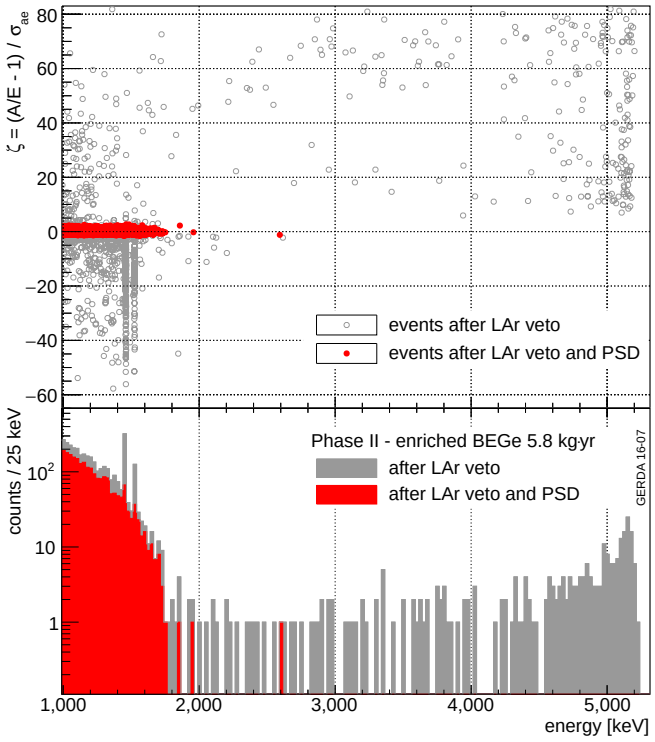

FIG. 3. — *pulse shape discrimination* — For all BEGe detectors, PSD parameter $\zeta = (A/E - 1)/\sigma_{ae}$ versus energy for physics data and the projection to the energy axis. Red circles and red spectrum represent events that pass the selection. Since the cuts are detector specific the accepted ζ ranges differ.

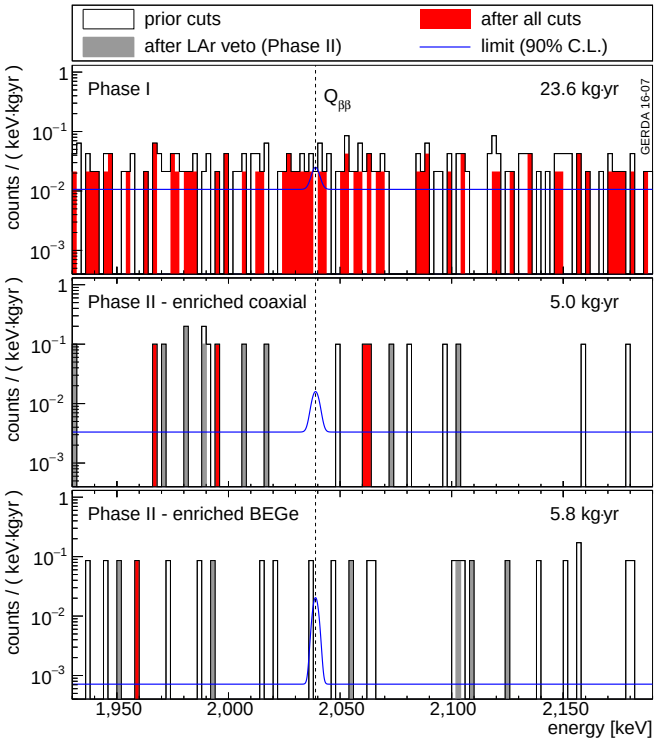

FIG. 4. — *energy spectra in the analysis window around* $Q_{\beta\beta}$ — Combined Phase I data (top), Phase II coaxial (middle) and BEGe detector spectra (bottom) in the analysis window. The binning is 2 keV. The exposures are given in the panels. The red histogram is the final spectrum, the filled grey one without PSD and the open one without PSD and without argon veto cut. The blue line represents the fitted spectrum together with a hypothetical signal corresponding to the 90 % C.L. limit of $T^{0\nu}_{1/2} = 5.3 \cdot 10^{25}$ yr.

achievement since the value is consistent with our ambitious design goal. We find no hint for a $0\nu\beta\beta$ decay signal in our combined data and place a limit of $T^{0\nu}_{1/2}(^{76}\mathrm{Ge}) > 5.3 \cdot 10^{25}$ yr (90 % C.L., sensitivity $4.0 \cdot 10^{25}$ yr). For light Majorana neutrino exchange and a nuclear matrix element range for ^{76}Ge between 2.8 and 6.1 [34–40] the GERDA half-life limit converts to $m_{\beta\beta}$ <0.15–0.33 eV (90 % C.L.).

The mean expected background is 0.8 in the energy region of interest at design exposure of 100 kg·yr; i.e. smaller than one. GERDA is hence the first "background-free" experiment in the field. Therefore, the sensitivity grows approximately linearly with exposure, unlike for competing experiments where the sensitivity grows with the square root of exposure. GERDA will reach a sensitivity in the order of 10^{26} yr for the half-life within 3 years of continuous operation. With the same exposure we have a 50 % chance to detect a signal with 3σ significance if the half-life is almost 10^{26} yr.

Phase II has demonstrated that the concept of background suppression by exploiting the good pulse shape performance of BEGe detectors and by detecting the argon scintillation light works. The background at $Q_{\beta\beta}$ is at a world-best level: it is lower by typically a factor of 10 compared to experiments using other isotopes after normalization by the energy resolution and total efficiency ϵ; i.e. (BI·FWHM/ϵ) is superior. This is the reason why the GERDA half-life sensitivity of $4.0 \cdot 10^{25}$ yr for an exposure of 343 mol·yr is similar to the one of Kamland-Zen for ^{136}Xe of $5.6 \cdot 10^{25}$ yr based on a more than 10-fold exposure of 3700 mol·yr [9].

A discovery of $0\nu\beta\beta$ decay would have far reaching consequences for our understanding of particle physics and cosmology. Key features for a convincing case are an ultra low background with a simple flat distribution, excellent energy resolution and the possibility to identify the events with high confidence as signal-like as opposed to an unknown γ line from a nuclear transition. The latter is achieved by the detector pulse shape analysis and possibly a signature in the argon. The concept to operate bare germanium detectors in liquid argon has proven to have the best performance for a discovery which motivates future extensions of the program. The GERDA cryostat can hold 200 kg of detectors. Such an experiment will remain "background-free" until an exposure of 1000 kg·yr provided the background can be further re-

duced by a factor of five. The discovery sensitivity would then improve by an order of magnitude to a half-life of 10^{27} yr. The 200 kg setup is conceived as a first step for a more ambitious 1 ton experiment which would ultimately boost the sensitivity to 10^{28} yr corresponding to the $m_{\beta\beta}$ <10–20 meV range. Both extensions are pursued by the newly formed LEGEND collaboration.

References

[a] Correspondence: gerda-eb@mpi-hd.mpg.de
[b] deceased
[c] also at: Dubna State University, Dubna, Russia
[d] also at: Moscow Inst. of Physics and Technology, Moscow, Russia

[1] S. Davidson, E. Nardi, and Y. Nir, *Leptogenesis*, Phys. Rep. **446** (2008) 105-177.

[2] R. N. Mohapatra and A. Y. Smirnov, *Neutrino mass and new physics*, Ann. Rev. Nucl. Part. Sci. **56** (2006) 569-628.

[3] R. N. Mohapatra *et al.*, *Theory of neutrinos: A white paper*, Rep. Prog. Phys. **70** (2007) 1757-1867.

[4] H. Päs and W. Rodejohann, *Neutrinoless double beta decay*, New J. Phys. **17** (2015) 115010.

[5] GERDA collaboration, M. Agostini *et al.*, *Results on Neutrinoless Double-β Decay of ^{76}Ge from Phase I of the* GERDA *Experiment*, Phys. Rev. Lett. **111** (2013) 122503.

[6] C. Cuesta *et al.*, *Status of the Majorana Demonstrator*, AIP Conf. Proc. **1686** (2015) 020005.

[7] K. Alfonso *et al.*, *Search for Neutrinoless Double-Beta Decay of ^{130}Te with CUORE-0*, Phys. Rev. Lett. **115** (2015) 102502.

[8] S. Andringa *et al.*, *Current Status and Future Prospects of the SNO+ Experiment*, Adv. High Energy Phys. **2016** (2016) 6194250.

[9] A. Gando *et al.*, *Search for Majorana Neutrinos near the Inverted Mass Hierarchy region with KamLAND-Zen*, Phys. Rev. Lett. **117** (2016) 082503.

[10] J.B. Albert *et al.*, *Search for Majorana neutrinos with the first two years of EXO-200 data*, Nature **510** (2014) 229-234.

[11] J. Martin-Albo *et al.*, *Sensitivity of NEXT-100 to neutrinoless double beta decay*, JHEP **1605** (2016) 159.

[12] B. J. Mount, M. Redshaw, and E. G. Myers, *Double-β-decay Q values of ^{74}Se and ^{76}Ge*, Phys. Rev. C **81** (2010) 032501.

[13] GERDA collaboration, K.-H. Ackermann *et al.*, *The* GERDA *experiment for the search of $0\nu\beta\beta$ decay in ^{76}Ge*, Eur. Phys. J. C **73** (2013) 2330.

[14] G. Heusser, *Low-radioactivity background techniques*, Ann. Rev. Nucl. Part. Sci. **45** (1995) 543-590.

[15] H. V. Klapdor-Kleingrothaus *et al.*, *Search for neutrinoless double beta decay with enriched ^{76}Ge in Gran Sasso 1990-2003*, Phys. Lett. B **586** (2004) 198-212.

[16] C. E. Aalseth *et al.*, *IGEX ^{76}Ge neutrinoless double beta decay experiment: Prospect for next generation experiments*, Phys. Rev. D **65** (2002) 092007.

[17] M. Agostini *et al.*, *Production, characterization and operation of ^{76}Ge enriched BEGe detectors in* GERDA, Eur. Phys. J. C **75** (2015) 39.

[18] GERDA collaboration, M. Agostini *et al.*, *The background in the $0\nu\beta\beta$ experiment* GERDA, Eur. Phys. J. C **74** (2014) 2764.

[19] S. Riboldi *et al.*, *Cryogenic readout techniques for Germanium detectors*, Conference procs. ANIMMA, doi:10.1109/ANIMMA.2015.7465549, 2015.

[20] M. Agostini *et al.*, *LArGe: active background suppression using argon scintillation for the Gerda $0\nu\beta\beta$-experiment*, Eur. Phys. J. C **75** (2015) 506.

[21] J. Janicskó Csáthy *et al.*, *Optical fiber read-out for liquid argon scintillation light*, arxiv:1606.04254, unpublished 2016.

[22] K. Freund *et al.*, *The performance of the Muon Veto of the* GERDA *experiment*, Eur. Phys. J. C **76** (2016) 1876.

[23] M. Agostini, L. Pandola and P. Zavarise, *Off-line data processing and analysis for the GERDA experiment*, J. Phys.: Conf. Ser. **368** (2012) 012047.

[24] M. Agostini *et al.*, *GELATIO: a general framework for modular digital analysis of high-purity Ge detector signals*, JINST **6** (2011) P08013.

[25] GERDA collaboration, M. Agostini *et al.*, *Improvement of the energy resolution via an optimized digital signal processing in* GERDA *Phase I*, Eur. Phys. J. C **75** (2015) 255.

[26] GERDA collaboration, M. Agostini, *et al.*, *Results on ββ decay with emission of two neutrinos or Majorons in ^{76}Ge from* GERDA *Phase I*, Eur. Phys. J. **C 75** (2015) 416.

[27] GERDA collaboration, M. Agostini *et al.*, *Pulse shape discrimination for* GERDA *Phase I data*, Eur. Phys. J. C **73** (2013) 2583.

[28] D. Budjáš *et al.*, *Pulse shape discrimination studies with a Broad-Energy Germanium detector for signal identification and background suppression in the* GERDA *double beta decay experiment*, JINST **4** (2009) P10007.

[29] M. Agostini *et al.*, *Signal modeling of high-purity Ge detectors with a small read-out electrode and application to neutrinoless double beta decay search in Ge-76*, JINST **6** (2011) P03005.

[30] V. Wagner, *Pulse Shape Analysis for the* GERDA *Experiment to Set a New Limit on the Half-life of $0\nu\beta\beta$ Decay of ^{76}Ge*, PhD thesis, MPI-K and U. Heidelberg, 2016.

[31] A. Kirsch, *Search for the neutrinoless double β-decay in* GERDA *Phase I using a Pulse Shape Discrimination technique*, PhD thesis, http://www.ub.uni-heidelberg.de/archiv/17149, MPI-K and U. Heidelberg, 2014.

[32] B. Bruyneel, B. Birkenbach, and P. Reiter, *Pulse shape analysis and position determination in segmented HPGe detectors: The AGATA detector library*, Eur. Phys. J. A **52** (2016) 70.

[33] GERDA collaboration, M. Agostini *et al.*, *Limit on neutrinoless double beta decay of ^{76}Ge by* GERDA, Physics Procedia **61** (2015) 828-837.

[34] J. Menendez *et al.*, *Disassembling the Nuclear Matrix Elements of the Neutrinoless beta beta Decay*, Nucl. Phys. A **818** (2009) 139-151.

[35] M. Horoi and A. Neacsu, *Shell model predictions for ^{124}Sn double-β decay*, Phys. Rev. C rr**93** (2016) 024308.

[36] J. Barea, J. Kotila, and F. Iachello, *$0\nu\beta\beta$ and $2\nu\beta\beta$ nuclear matrix elements in the interacting boson model with isospin restoration*, Phys. Rev. C **91** (2015) 034304.

[37] J. Hyvärinen and J. Suhonen, *Nuclear matrix elements for $0\nu\beta\beta$ decays with light or heavy Majorana-neutrino exchange*, Phys. Rev. C **91** (2015) 024613.
[38] F. Simkovic *et al.*, *$0\nu\beta\beta$ and $2\nu\beta\beta$ nuclear matrix elements, quasiparticle random-phase approximation, and isospin symmetry restoration*, Phys. Rev. C. **87** (2013) 045501.
[39] N. Lopez Vaquero, T.R. Rodriguez, and J.L. Egido, *Shape and pairing fluctuation effects on neutrinoless double beta decay nuclear matrix elements*, Phys. Rev. Lett. **111** (2013) 142501.
[40] J. Yao *et al.*, *Systematic study of nuclear matrix elements in neutrinoless double-beta decay with a beyond-mean-field covariant density functional theory*, Phys. Rev. C **91** (2015) 024316.
[41] GERDA collaboration, M. Agostini *et al.*, *Upgrade of the* GERDA *Experiment*, Proceedings of Science (TIPP2014) 109, 2014.
[42] J. Beringer *et al.*, *Review of Particle Physics*, Phys. Rev. **D86** (2012) 010001.
[43] G. Cowan *et al.*, *Asymptotic formulae for likelihood-based tests of new physics*, Eur. Phys. J. C **71** (2011) 1554.
[44] G. J. Feldman and R. D. Cousins, *A Unified approach to the classical statistical analysis of small signals*, Phys. Rev. D **57** (1998) 3873-3889
[45] A. Caldwell, D. Kollar, and K. Kröninger, *BAT - The Bayesian Analysis Toolkit*, Comput. Phys. Commun.**180** (2009) 2197-2209.
[46] R. Cousins and V. Highland, *Incorporating systematic uncertainties into an upper limit*, Nucl. Instr. Meth. A**320** (1992) 331-335.
[47] S. V. Biller and S. M. Oser, *Another look at confidence intervals: Proposal for a more relevant and transparent approach*, Nucl. Instr. Meth. A**774** (2015) 103-119.

Acknowledgments

The GERDA experiment is supported financially by the German Federal Ministry for Education and Research (BMBF), the German Research Foundation (DFG) via the Excellence Cluster Universe, the Italian Istituto Nazionale di Fisica Nucleare (INFN), the Max Planck Society (MPG), the Polish National Science Centre (NCN), the Russian Foundation for Basic Research (RFBR), and the Swiss National Science Foundation (SNF). The institutions acknowledge also internal financial support.

The GERDA collaboration thanks the directors and the staff of the LNGS for their continuous strong support of the GERDA experiment.

Author Contributions

All authors have contributed to the publication, being differently involved in the design and construction of the detector system, in its operation, and in the acquisition and analysis of data. All authors approved the final version of the manuscript. In line with collaboration policy, the authors are listed here alphabetically. GERDA was constructed and commissioned by the authors of Refs. [13] and [41].

Author Information

The GERDA collaboration website is found at `https://www.mpi-hd.mpg.de/gerda/`

Extended Method Section

This section discusses the statistical analysis of the GERDA data. In particular, the procedures to derive the limit on $T^{0\nu}_{1/2}$, the median sensitivity of the experiment and the treatment of systematic uncertainties are described.

A combined analysis of data from Phase I and II is performed by fitting simultaneously the six data sets of Table I. The parameter of interest for this analysis is the strength of a possible $0\nu\beta\beta$ decay signal: $\mathcal{S} = 1/T^{0\nu}_{1/2}$. The number of expected $0\nu\beta\beta$ events in the i-th data set $\mathcal{D}_i$ as a function of $\mathcal{S}$ is given by:

$$\mu_i^S = \ln 2 \cdot (N_A/m_a) \cdot \epsilon_i \cdot \mathcal{E}_i \cdot \mathcal{S} \ , \tag{2}$$

where N_A is Avogadro's number, ϵ_i the global signal efficiency of the i-th data set, $\mathcal{E}_i$ the exposure and m_a the molar mass. The exposure quoted is the total detector mass multiplied by the data taking time. The global signal efficiency accounts for the fraction of ^{76}Ge in the detector material, the fraction of the detector active volume, the efficiency of the analysis cuts, the fractional live time of the experiment and the probability that $0\nu\beta\beta$ decay events in the active detector volume have a reconstructed energy at $Q_{\beta\beta}$. The total number of expected background events as a function of the background index BI_i is:

$$\mu_i^B = \mathcal{E}_i \cdot \mathrm{BI}_i \cdot \Delta E, \tag{3}$$

where ΔE=240 keV is the width of the energy region around $Q_{\beta\beta}$ used for the fit.

Each data set $\mathcal{D}_i$ is fitted with an unbinned likelihood function assuming a Gaussian distribution for the signal and a flat distribution for the background:

$$\mathcal{L}_i(\mathcal{D}_i|\mathcal{S},\mathrm{BI}_i,\theta_i) \ = \ \frac{1}{\mu_i^S+\mu_i^B}\cdot \prod_{j=1}^{N_i^{obs}}\left[\mu_i^S\cdot\frac{1}{\sqrt{2\pi}\sigma_i}\exp\left(\frac{-(E_j-Q_{\beta\beta}-\delta_i)^2}{2\sigma_i^2}\right)+\mu_i^B\cdot\frac{1}{\Delta E}\right] \tag{4}$$

where E_j are the individual event energies, N_i^{obs} is the total number of events observed in the i-th data set, $\sigma_i = \mathrm{FWHM}_i/(2\sqrt{2\ln 2})$ is the energy resolution and δ_i is a possible systematic energy offset. The parameters with systematic uncertainties are indicated with $\theta_i = \{\epsilon_i, \sigma_i, \delta_i\}$. The parameters $\mathcal{S}$ and BI_i are bound to positive values. The total likelihood is constructed as the product of all $\mathcal{L}_i$ weighted with the Poisson terms [42]:

$$\mathcal{L}(\boldsymbol{\mathcal{D}}|\mathcal{S},\mathbf{BI},\boldsymbol{\theta}) = \prod_i\left[\frac{e^{-(\mu_i^S+\mu_i^B)}\cdot(\mu_i^S+\mu_i^B)^{N_i^{obs}}}{N_i^{obs}!}\cdot\mathcal{L}_i(\mathcal{D}_i|\mathcal{S},\mathrm{BI}_i,\theta_i)\right] \tag{5}$$

where $\boldsymbol{\mathcal{D}} = \{\mathcal{D}_1 \dots \mathcal{D}_i \dots\}$, $\mathbf{BI} = \{\mathrm{BI}_1 \dots \mathrm{BI}_i \dots\}$ and $\boldsymbol{\theta} = \{\theta_1 \dots \theta_i \dots\}$.

A frequentist analysis is performed using a two-sided test statistics [43] based on the profile likelihood λ ($\mathcal{S}$):

$$t_{\mathcal{S}} = -2\ln\lambda(\mathcal{S}) = -2\ln\frac{\mathcal{L}(\mathcal{S},\hat{\hat{\mathbf{BI}}},\hat{\hat{\boldsymbol{\theta}}})}{\mathcal{L}(\hat{\mathcal{S}},\hat{\mathbf{BI}},\hat{\boldsymbol{\theta}})} \tag{6}$$

where $\hat{\hat{\mathbf{BI}}}$ and $\hat{\hat{\boldsymbol{\theta}}}$ in the numerator denote the value of the parameters that maximizes $\mathcal{L}$ for a fixed $\mathcal{S}$. In the denominator, $\hat{\mathcal{S}}$, $\hat{\mathrm{BI}}$ and $\hat{\boldsymbol{\theta}}$ are the values corresponding to the absolute maximum likelihood.

The confidence intervals are constructed for a discrete set of values $\mathcal{S} \in \{\mathcal{S}_j\}$. For each $\mathcal{S}_j$, possible realizations of the experiments are generated via Monte Carlo according to the parameters of Table I and the expected number of counts from Eqs. 2 and 3. For each realization $t_{\mathcal{S}j}$ is evaluated. From the entire set the probability distribution $f(t_{\mathcal{S}}|\mathcal{S}_j)$ is calculated. The p-value of the data for a specific $\mathcal{S}_j$ is computed as:

$$p_{\mathcal{S}_j} = \int_{t_{obs}}^{\infty} f(t_{\mathcal{S}}|\mathcal{S}_j)\, d(t_{\mathcal{S}j}) \tag{7}$$

where t_{obs} is the value of the test statistics of the GERDA data for $\mathcal{S}_j$. The values of $p_{\mathcal{S}_j}$ are shown by the solid line in Extended Data Fig. 5. The 90 % C.L. interval is given by all $\mathcal{S}_j$ values with $p_{\mathcal{S}_j} > 0.1$. Such an interval has the correct coverage by construction. The current analysis yields a one-sided interval, i.e. a limit of $T^{0\nu}_{1/2} = 1/\mathcal{S} > 5.3\cdot 10^{25}$ yr.

The expectation for the frequentist limit (i.e. the experimental sensitivity) was evaluated from the distribution of $p_{\mathcal{S}_j}$ built from Monte Carlo generated data sets with no injected signal ($\mathcal{S} = 0$). The distribution of $p_{\mathcal{S}_j}$ is shown in Extended Data Fig. 5: the dashed line is the median of the distribution and the color bands indicate the 68 % and 90 % probability central intervals. The experimental sensitivity corresponds to the $\mathcal{S}$ value at which the median crosses the p-value threshold of 0.1 : $T^{0\nu}_{1/2} > 4.0\cdot 10^{25}$ yr (90% C.L.).

Systematics uncertainties are folded into the likelihood by varying the parameters θ_i in the fits and constraining them by adding to the likelihood multiplicative Gaussian penalty terms. The central values and the standard deviations of the penalty terms for ϵ_i and σ_i are taken from Table I. The penalty term on δ_i has a central value equal to zero and standard deviation of 0.2 keV.

Instead of the two-sided test statistics one can use a one-sided test statistic defined as [43]:

$$\tilde{t}_{\mathcal{S}} = \begin{cases} 0, & \hat{\mathcal{S}} > \mathcal{S} \geq 0 \\ -2\ln\lambda(\mathcal{S}), & \hat{\mathcal{S}} \leq \mathcal{S} \end{cases} \tag{8}$$

By construction $\tilde{t}_{\mathcal{S}} = 0$ for $\mathcal{S} = 0$ for all realizations and consequently $\mathcal{S} = 0$ is always included in the 90 %

C.L. interval, i.e. the one-sided test statistic will always yield a limit. In our case the resulting limit would be 50% stronger. Similar to other experiments [9, 10], we want to be able to detect a possible signal and thus we decided a priori to adopt the two-sided test statistic. It is noteworthy that, although the coverage of both test statistics is correct by construction, deciding which one to use according to the outcome of the experiment would result in the flip-flop issue discussed by Feldman and Cousins [44].

The statistical analysis is also performed within a Bayesian framework. The combined posterior probability density function (PDF) is calculated from the six data sets according to Bayes' theorem:

$$\mathcal{P}(\mathcal{S}, \mathbf{BI}|\boldsymbol{\mathcal{D}}, \boldsymbol{\theta}) \propto \mathcal{L}(\boldsymbol{\mathcal{D}}|\mathcal{S}, \mathbf{BI}, \boldsymbol{\theta})\ \mathcal{P}(\mathcal{S})\ \prod_i \mathcal{P}(\mathrm{BI}_i) \quad (9)$$

The likelihood $\mathcal{L}$ is given by Eq. (5), while $\mathcal{P}(\mathcal{S})$ and $\mathcal{P}(\mathrm{BI}_i)$ are the prior PDFs for $\mathcal{S}$ and for the background indices, respectively. The one-dimensional posterior PDF $\mathcal{P}(\mathcal{S}|\boldsymbol{\mathcal{D}}, \boldsymbol{\theta})$ of the parameter $\mathcal{S}$ of interest is derived by marginalization over all nuisance parameters **BI**. The marginalization is performed by the BAT toolkit [45] via a Markov chain Monte Carlo numerical integration. A flat PDF between 0 and 0.1 cts/(keV · kg · yr) is considered as prior for all background indices. As in Ref. [5], a flat prior distribution is taken for $\mathcal{S}$ between 0 and 10^{-24} /yr, i.e. all counting rates up to a maximum are considered to be equiprobable. The parameters $\boldsymbol{\theta}$ in the likelihood $\mathcal{L}$ are fixed during the Bayesian analysis and the uncertainties are folded into the posterior PDF as last step by an integral average:

$$\langle \mathcal{P}(\mathcal{S}|\boldsymbol{\mathcal{D}}) \rangle = \int \mathcal{P}(\mathcal{S}|\boldsymbol{\mathcal{D}}, \boldsymbol{\theta}) \prod_i g(\theta_i) d\theta_i \quad (10)$$

with $g(\theta_i)$ being Gaussian distributions like for the frequentist analysis. The integration is performed numerically by a Monte Carlo approach.

The median sensitivity of the experiment in the case of no signal is $T^{0\nu}_{1/2} > 3.1 \cdot 10^{25}$ yr (90% C.I.). The posterior PDF $\langle \mathcal{P}(\mathcal{S}|\boldsymbol{\mathcal{D}}) \rangle$ for our data has an exponential shape with the mode at $\mathcal{S} = 0$. Its 90 % probability quantile yields $T^{0\nu}_{1/2} > 3.5 \cdot 10^{25}$ yr.

As in any Bayesian analysis, results depend on the choice of the priors. For our limit we assume all signal count rates to be a priori equiprobable. Alternative reasonable choices are for instance: equiprobable Majorana neutrino masses, which yields a prior proportional to $1/\sqrt{\mathcal{S}}$; or scale invariance in the counting rate, namely a flat prior in $\log(\mathcal{S})$. The limits derived with these assumptions are significantly stronger (50 % or more), since for both alternatives the prior PDFs increase the probability of low $\mathcal{S}$ values.

The systematic uncertainties weaken the limit on $\mathcal{S}$ by less than 1% both in the frequentist and Bayesian analysis. In general, the impact of systematic uncertainties on limits is marginal in the low-statistics regime that characterizes our experiment (see also Ref. [46]).

The limit derived from the GERDA data is slightly stronger than the median sensitivity. This effect is more significant in the frequentist analysis as one would expect, see e.g. Ref. [47] for a detailed discussion. The probability of obtaining a frequentist (Bayesian) limit stronger than the actual one is 33 % (35 %).

Extended Data Figures

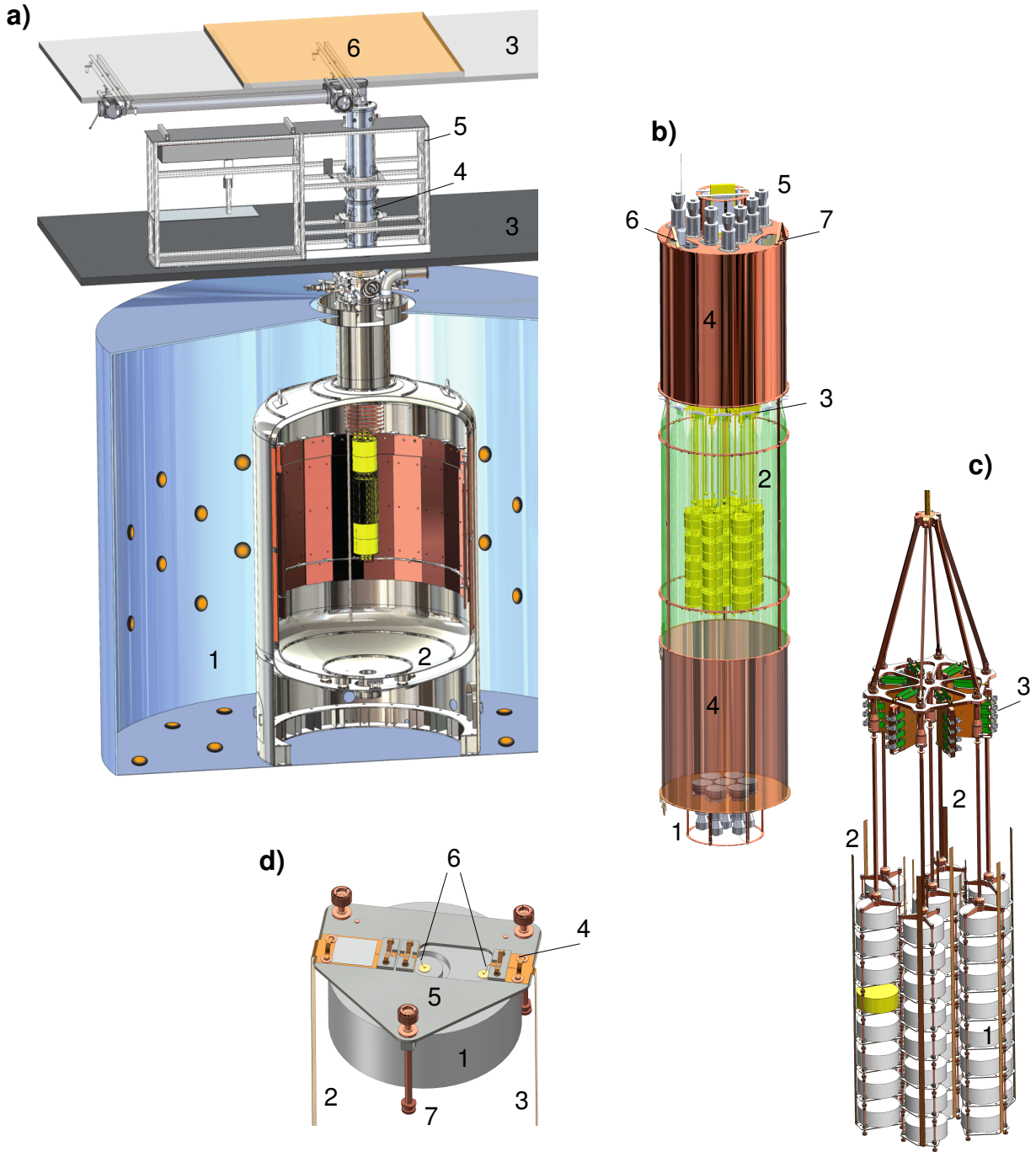

Extended Data Fig. 1. — GERDA *Phase II experimental setup.* —
a) overview: (1) water tank with muon veto system PMTs (590 m^3, diameter 10 m), (2) LAr cryostat (64 m^3, diameter 4 m), (3) floor & roof of clean room, (4) lock, (5) glove box, (6) plastic muon veto system;
b) LAr veto system: (1/5) bottom/top plate (diameter 49 cm) with 7/9 3" PMTs (R11065-10/20 MOD) with low radioactivity of U and Th (<2 mBq/PMT), (2) fiber curtain (height 90 cm) coated with wavelength shifter, (3) optical couplers and SiPMs, (4) thin-walled (0.1 mm) Cu cylinders (height 60 cm) covered with a Tyvek reflector on the inside, (6) calibration source entering slot in top plate, (7) slot for second of three calibration sources;
c) detector array: (1) Ge detectors arranged in 7 strings, (2) flexible bias and readout cables, (3) amplifiers;
d) detector module, view from bottom: (1) BEGe diode, (2/3) signal/high voltage cables attached by (4) bronze clamps to (5) silicon support plate, (6) bond wire connections from diode to signal and high voltage cable, (7) Cu support rods.

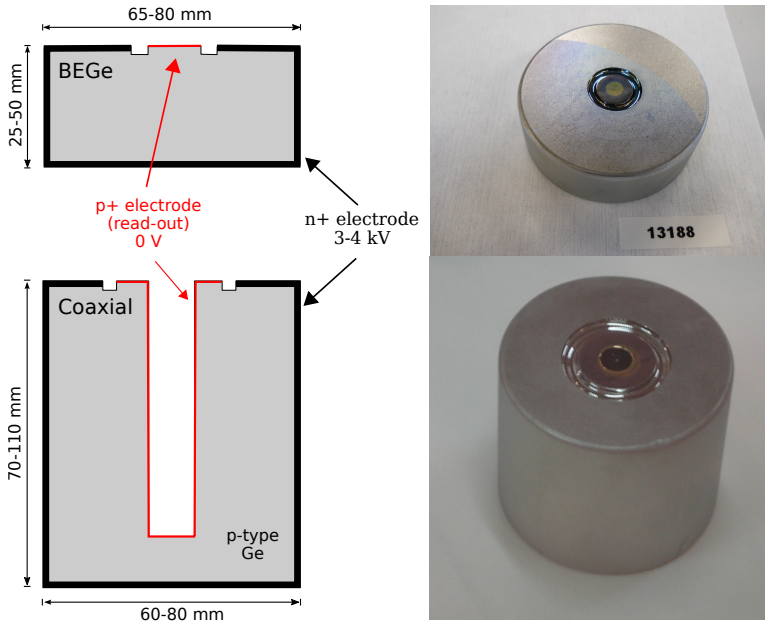

Extended Data Fig. 2. — *detector types* — Cross section through the germanium detector types (left) and the corresponding photos of them (right). The p+ electrode is made by a ∼0.3 µm thin boron implantation. The n+ electrode is a 1-2 mm thick lithium diffusion layer and biased with up to +4500 V. The electric field drops to zero in the n+ layer and hence energy depositions in this fraction of the volume do not create a readout signal. The p+ electrode is connected to a charge sensitive amplifier.

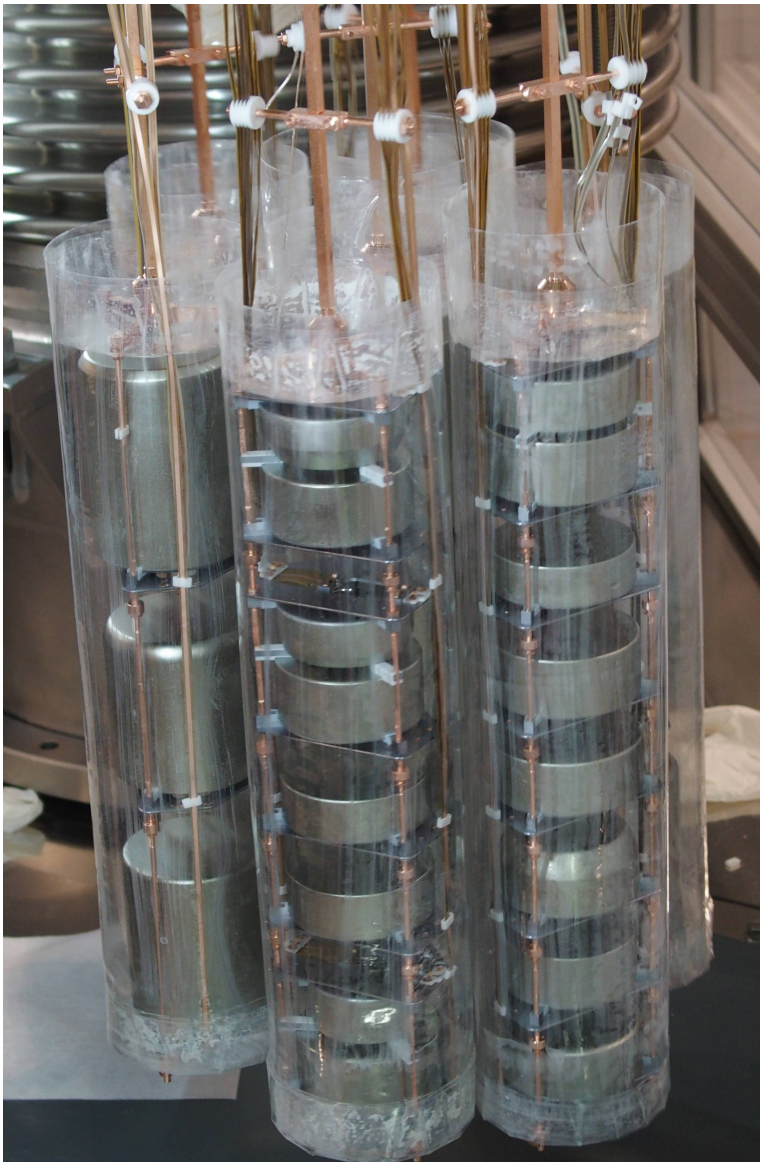

Extended Data Fig. 3. — *GERmanium Detector Array* GERDA — Photo of the assembled detector array with a string of coaxial detectors (left) and BEGe detectors (middle and right). Each string is enclosed by a cylindrical nylon shroud covered with a wavelength shifter.

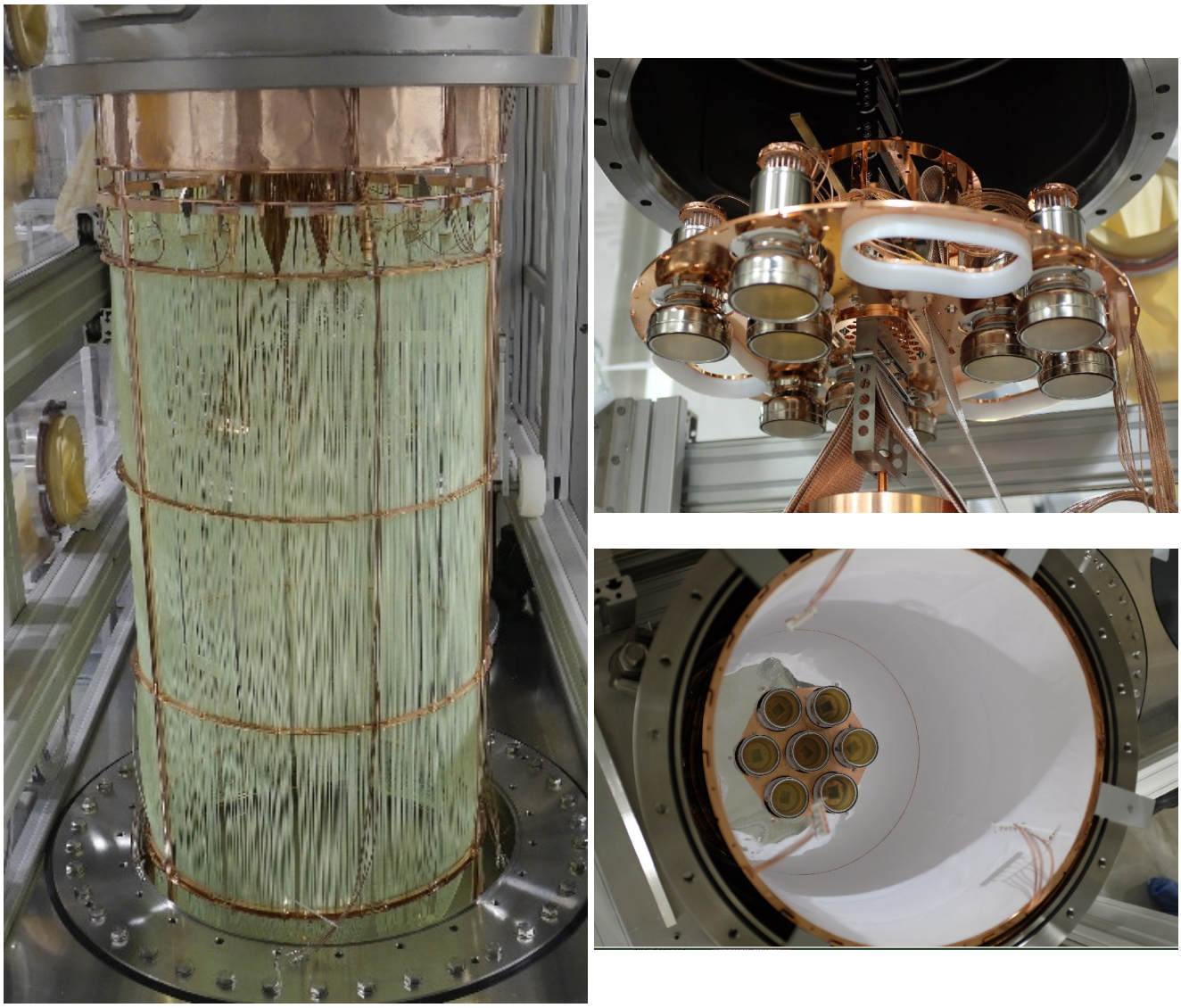

Extended Data Fig. 4. — *liquid Argon veto* — Photos of the liquid argon veto system. Left: fiber curtain with SiPM readout at the top. Right: top and bottom arrangement of PMTs.

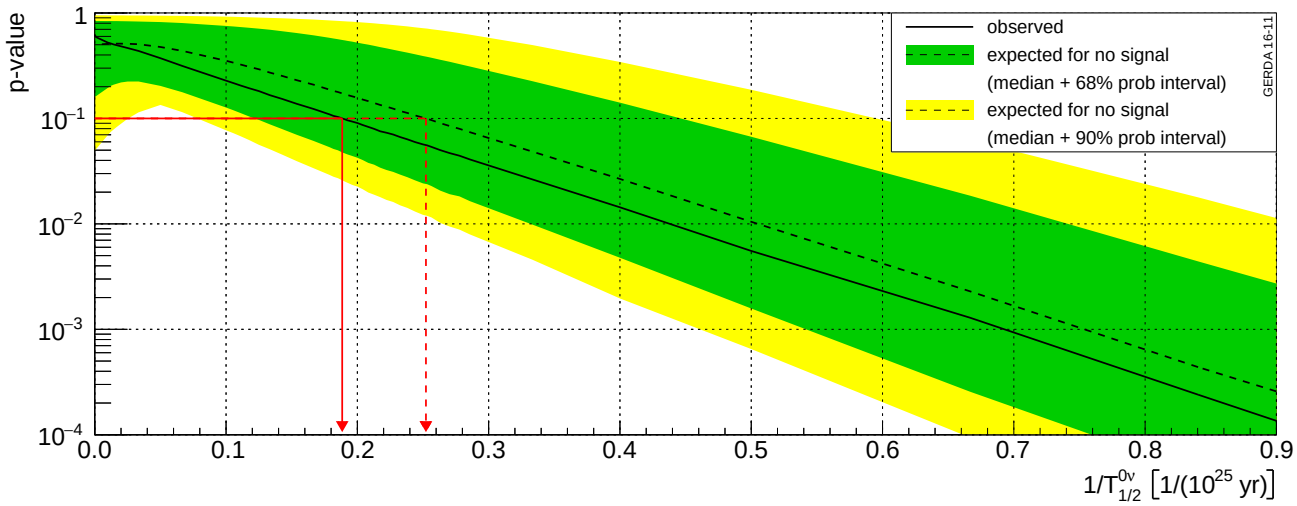

Extended Data Fig. 5. — *frequentist hypothesis test* — p-value for the hypothesis test as a function of the inverse half-life $1/T^{0\nu}_{1/2}$ according to Eq. 7 of the Extended Method Section. The color bands indicate for many Monte Carlo realizations according to the GERDA parameters (with no signal) the spread of the p-value distributions: in green and yellow for the central 68 % and 90 % probability intervals, respectively. The dashed black line represents the median of the distribution; the p-value for the GERDA data is shown as solid black line. The red arrows indicate the results at 90 % confidence level, i.e. a p-value of 0.1: the limit for $T^{0\nu}_{1/2}(^{76}\mathrm{Ge}) > 5.3 \cdot 10^{25}$ yr (full red arrow), and the median sensitivity for $T^{0\nu}_{1/2}(^{76}\mathrm{Ge}) > 4.0 \cdot 10^{25}$ yr (dashed red arrow). For a detailed discussion of their computation see the Extended Method section.

Data Availabilty

All data generated during this analysis and shown in Figs. 1 to 4 are available in ASCII format (CSV) from the GERDA home page (https://www.mpi-hd.mpg.de/gerda/public/index.html) or from Nature as they are included in this published article (and its supplementary information files). For further information contact the GERDA Editorial Board (gerda-eb@mpi-hd.mpg.de).

List of Figures

1. — *energy scale and resolution* — Average energy resolution (FWHM) for γ lines of the calibration spectrum (filled symbols) and for the average of ^{40}K and ^{42}K lines from physics data (open symbols) for BEGe (symbols and solid line in blue) and coaxial (symbols and dashed line in red) detectors; the uncertainties ($\pm$1 s.d.) are derived from the fit. The insets show the potassium lines and the 2615 keV calibration peak.
2. — *energy spectra for the two detector types* — Energy spectra of Phase II data sets before (open histogram) and after argon veto cut (filled histogram). The blue lines are the expected $2\nu\beta\beta$ spectra from our recent half-life measurement. The inset shows the BEGe spectrum in the energy region around the two potassium lines. Note, the ^{40}K line is not suppressed since no energy is deposited in the LAr. Various background contributions are labeled in the bottom panel.
3. — *pulse shape discrimination* — For all BEGe detectors, PSD parameter $\zeta = (A/E - 1)/\sigma_{ae}$ versus energy for physics data and the projection to the energy axis. Red circles and red spectrum represent events that pass the selection. Since the cuts are detector specific the accepted ζ ranges differ.
4. — *energy spectra in the analysis window around* $Q_{\beta\beta}$ — Combined Phase I data (top), Phase II coaxial (middle) and BEGe detector spectra (bottom) in the analysis window. The binning is 2 keV. The exposures are given in the panels. The red histogram is the final spectrum, the filled grey one without PSD and the open one without PSD and without argon veto cut. The blue line represents the fitted spectrum together with a hypothetical signal corresponding to the 90 % C.L. limit of $T^{0\nu}_{1/2} = 5.3 \cdot 10^{25}$ yr.

Extended Figures

1. — GERDA *Phase II experimental setup.* —
a) overview: (1) water tank with muon veto system PMTs (590 m^3, diameter 10 m), (2) LAr cryostat (64 m^3, diameter 4 m), (3) floor & roof of clean room, (4) lock, (5) glove box, (6) plastic muon veto system;
b) LAr veto system: (1/5) bottom/top plate (diameter 49 cm) with 7/9 3" PMTs (R11065-10/20 MOD) with low radioactivity of U and Th (<2 mBq/PMT), (2) fiber curtain (height 90 cm) coated with wavelength shifter, (3) optical couplers and SiPMs, (4) thin-walled (0.1 mm) Cu cylinders (height 60 cm) covered with a Tyvek reflector on the inside, (6) calibration source entering slot in top plate, (7) slot for second of three calibration sources;
c) detector array: (1) Ge detectors arranged in 7 strings, (2) flexible bias and readout cables, (3) amplifiers;
d) detector module, view from bottom: (1) BEGe diode, (2/3) signal/high voltage cables attached by (4) bronze clamps to (5) silicon support plate, (6) bond wire connections from diode to signal and high voltage cable, (7) Cu support rods.
2. — *detector types* — Cross section through the germanium detector types (left) and the corresponding photos of them (right). The p+ electrode is made by a $\sim$0.3 µm thin boron implantation. The n+ electrode is a 1-2 mm thick lithium diffusion layer and biased with up to +4500 V. The electric field drops to zero in the n+ layer and hence energy depositions in this fraction of the volume do not create a readout signal. The p+ electrode is connected to a charge sensitive amplifier.
3. — *GERmanium Detector Array* GERDA — Photo of the assembled detector array with a string of coaxial detectors (left) and BEGe detectors (middle and right). Each string is enclosed by a cylindrical nylon shroud covered with a wavelength shifter.
4. — *liquid Argon veto* — Photos of the liquid argon veto system. Left: fiber curtain with SiPM readout at the top. Right: top and bottom arrangement of PMTs.
5. — *frequentist hypothesis test* — p-value for the hypothesis test as a function of the inverse half-life $1/T^{0\nu}_{1/2}$ according to Eq. 7 of the Extended Method Section. The color bands indicate for many Monte Carlo realizations according to the GERDA parameters (with no signal) the spread of the p-value distributions: in green and yellow for the central 68 % and 90 % probability intervals, respectively. The dashed black line represents the median of the distribution; the p-value for the GERDA data is shown as solid black line. The red arrows indicate the results at 90 % confidence level, i.e. a p-value of 0.1: the limit for $T^{0\nu}_{1/2}(^{76}\mathrm{Ge}) > 5.3 \cdot 10^{25}$ yr (full red arrow), and the median sensitivity for $T^{0\nu}_{1/2}(^{76}\mathrm{Ge}) > 4.0 \cdot 10^{25}$ yr (dashed red arrow). For a detailed discussion of their computation see the Extended Method section.